

## Self-similar hierarchical honeycombs

Babak Haghpanah, Ramin Oftadeh, Jim Papadopoulos and Ashkan Vaziri

*Proc. R. Soc. A* 2013 **469**, 20130022, published 5 June 2013

---

### References

**This article cites 34 articles, 8 of which can be accessed free**  
<http://rspa.royalsocietypublishing.org/content/469/2156/20130022.full.html#ref-list-1>

### Subject collections

Articles on similar topics can be found in the following collections  
[mechanical engineering](#) (164 articles)

### Email alerting service

Receive free email alerts when new articles cite this article - sign up in the box at the top right-hand corner of the article or click [here](#)

## Research



CrossMark  
click for updates

**Cite this article:** Haghpanah B, Oftadeh R, Papadopoulos J, Vaziri A. 2013 Self-similar hierarchical honeycombs. *Proc R Soc A* 469: 20130022.

<http://dx.doi.org/10.1098/rspa.2013.0022>

Received: 14 January 2013

Accepted: 8 May 2013

### Subject Areas:

mechanical engineering

### Keywords:

structural hierarchy, honeycombs, cellular structures, plastic collapse, limit analysis

### Author for correspondence:

Ashkan Vaziri

e-mail: [vaziri@coe.neu.edu](mailto:vaziri@coe.neu.edu)

# Self-similar hierarchical honeycombs

Babak Haghpanah, Ramin Oftadeh,

Jim Papadopoulos and Ashkan Vaziri

Department of Mechanical and Industrial Engineering,  
Northeastern University, Boston, MA 02115, USA

Hierarchical structures are observed in nature, and can be shown to offer superior efficiency. However, the potential advantages of structural hierarchy are not well understood. We extensively explored a bending-dominated model material (i.e. transversely loaded hexagonal honeycomb) which is susceptible to improvement by simple iterative refinement that replaces each three-edge structural node with a smaller hexagon. Using a blend of analytical and numerical techniques, both elastic and plastic properties were explored over a range of loadings and iteration parameters. A wide variety of specific stiffness and specific strengths (up to fourfold increase) were achieved. The results offer insights into the potential value of iterative structural refinement for creating low-density materials with desired properties and function.

## 1. Introduction

Two-dimensional cellular structures (honeycombs) generally offer desirable out-of-plane mechanical properties, making them attractive candidates for applications, including thermal isolation, energy absorption, structural protection and as the core of lightweight sandwich panels [1–7]. The in-plane properties (e.g. stiffness, strength and energy absorption) of such structures are generally far inferior to their out-of-plane properties. There have been recent efforts, however, to use the low in-plane stiffness and auxetic properties of honeycombs in designing flexible structures for applications that require high deformation under targeted loads [8–10]. One example of such design using compliant, highly deformable honeycombs is flexible microelectro-mechanical-system structures [11–13], where it is difficult to use sliding or revolving joints (such as hinges and axes), mainly owing

to tribological issues, friction, wear and the low overall reliability of these elements. Micromechanisms, as a result, should be designed as compliant or flexible-link mechanisms [12,14,15]. Compliant honeycombs have also been suggested for use in microdevices as versatile motion transformers [12], microcapsules [16] and motion detectors [13]. One other example of such flexible design is the morphing structures in aircrafts using honeycombs with negative Poisson's ratio to control aeroelastic and structural performance of wings, blades and flexible skins in response to changing flight conditions [17–24]. Other applications for two-dimensional cellular solids benefiting from their unique in-plane properties are honeycombs as analogues of spokes in non-pneumatic tyres [25,26], molecular mechanisms [27], core of curved sandwich shells [28] and vibration absorbers for sandwich panels [29–31]. Considering these emerging applications requiring specific combinations of strength and stiffness or compliance, one goal of this study is to achieve a class of hierarchical structures with *tailorable* in-plane properties that allow for adjusting properties, based on functionality; for instance, lowering the value of stiffness while increasing strength to obtain a cellular material that is easily deformed but resistant to rupture, or increasing both stiffness and toughness to enhance the impact resistance and load-bearing capacity, etc.

In this context, we looked at a particular refinement scheme: replacing each three-edge node with a smaller, parallel hexagon. This procedure is iterative, in that it produces additional three-edge nodes that can likewise be replaced by even smaller hexagons. As such, it allows us to comprehensively explore iteration parameters and loadings, with the benefits and insights afforded by analytical machinery. The results are of interest in two ways: first, there is a possibility that the results we find could be of actual use to achieve some tailored combination of stiffness and strength. Second, we see this study as providing a conceptual model for ways of optimizing hierarchical structure, and for ideas of what kinds of improvements may be possible.

This iteratively refined structure is a type of *self-similar hierarchical honeycomb* capable of achieving higher specific in-plane uniaxial stiffness than the regular honeycomb [32]. The introduced hexagons may have a different wall thickness than the underlying grid, and an overall thickness re-scaling is used to maintain a fixed amount of material per unit area. This substitution can be iterated to generate ever-finer structural detail, while preserving both the structure's average density, and its sixfold symmetry (a sufficient condition for in-plane isotropy in the linear-elastic regime [33]). Figure 1 shows visual schematics and three-dimensionally printed samples of first- and second-order hierarchical honeycombs with uniform wall thickness. Such structures can exhibit an in-plane Young's modulus of up to two and 3.5 times that of regular hexagonal honeycomb structure of the same mass (density), respectively [32].

Here, we present investigations for the plastic collapse of hierarchical honeycombs where arbitrary normal stresses are applied along  $x$  (the so-called armchair or ribbon direction) and  $y$  (the so-called zigzag or transverse direction), without any  $xy$  shear loading (figure 2a). Analytical studies on plastic collapse are limited to hierarchical honeycombs with just one order of hierarchy, as additional refinement significantly increases the difficulties of analytical study. In finite-element investigations, we present results for hierarchical honeycombs with up to four orders of hierarchy for plastic collapse strength, as well as in-plane stiffness (i.e. effective Young's modulus). It should be emphasized that instability along with plastic collapse are the two general collapse mechanisms in cellular structures [34–37]. For example, for regular hexagonal honeycombs under in-plane biaxial loading along ribbon and armchair directions, instability could—based on the relative density of the structure—become the driving mechanism of collapse when both principal stresses are compressive. However, plastic collapse could be the failure mechanism under loadings where at least one of the principal stresses is tensile [37]. In this paper, we focus on studying the plastic collapse in hierarchical honeycombs, and additional studies are required to investigate their buckling behaviour.

Our analytical models of plastic collapse strength for first-order hierarchical honeycombs are based on upper- and lower-bound classical frame limit analyses [38,39] applied to a 'unit cell' of the periodic structure (in crystallographic terms, this is in fact one half of the true unit cell of the lattice). To establish their validity, we also carried out two kinds of finite-element

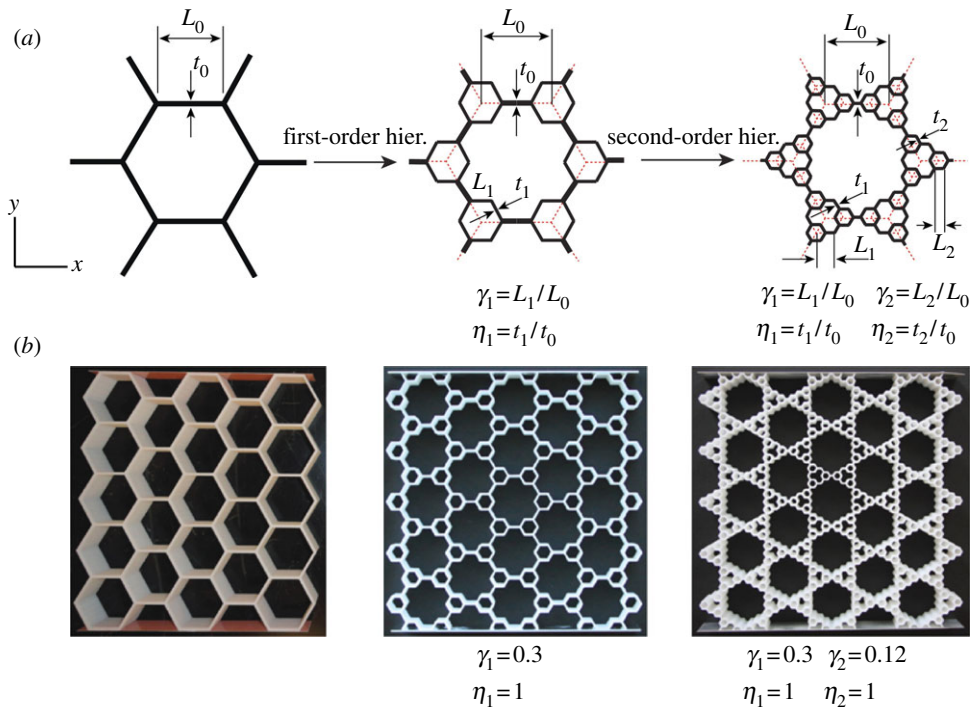


**Figure 1.** Hierarchical honeycombs. (a) Regular and hierarchical honeycombs with first- and second-order hierarchy. (b) Images of hierarchical honeycombs fabricated using three-dimensional printing. (Online version in colour.)

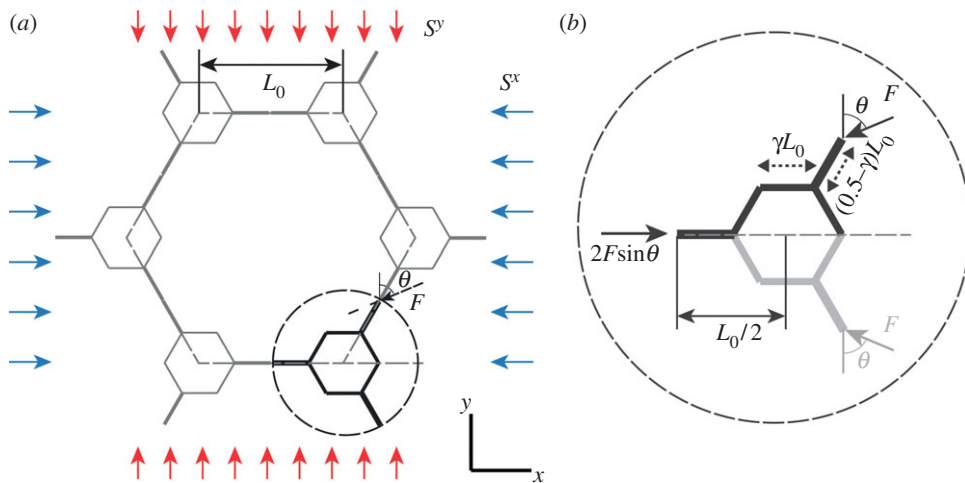


**Figure 2.** (a) A section of a first-order hierarchical honeycomb under biaxial loading, where the unit cell is marked by bold lines. (b) Free body diagram of the unit cell for both elastic and plastic analyses. Only half of the unit cell is analysed due to symmetry. (Online version in colour.)

simulations of unit-cell plasticity, using beam elements with elastic-perfectly plastic moment-curvature behaviour. Basic relations governing hierarchical honeycombs and the definition of a unit cell for biaxial ( $x - y$ ) loading are given in §2. Plastic collapse analysis methodology is described in §3. Details of the finite-element models are given in §4. The results are presented and

discussed in §5. First, results for first-order hierarchical honeycombs under uniaxial loading in either the  $x$ - or  $y$ -direction, including the comparison between analytical models and simulations, are presented in §5*a*. In §5*b*, the analytical collapse surface of a hierarchical honeycomb under biaxial ( $x - y$ ) loading is discussed, and compared with that of regular hexagonal honeycomb. In §5*c*, the trade-off between specific strength and specific stiffness for different first-order hierarchical honeycombs is discussed. Section 6 describes selected numerical results for stiffness and strength in hierarchical honeycombs with orders 1–4, showing that a wide range of stiffness and strength can be achieved by varying the hierarchical architecture of honeycombs. Concluding remarks are provided in §7.

## 2. Hierarchical honeycombs: basic unit-cell relations

Figure 1*a* shows a schematic of the geometrical substitutions resulting in first- and second-order hierarchical honeycombs. For each level  $i$  of hierarchy, two parameters, namely  $\gamma_i$  and  $\eta_i$ , are used to define the substitution geometry. The length ratio,  $\gamma_i$ , is defined as the ratio of the new hexagon side to the original hexagon side,  $L_0$ . The thickness ratio,  $\eta_i$ , is the ratio of new hexagon wall thickness to the wall thickness of the remaining parts of the original hexagons. (After a refinement step, this entire structure is reduced in thickness by a fixed fraction, while keeping all  $\eta_i$  constant, so the total mass remains unchanged.) For example, for the first-order hierarchy shown in figure 1*a*,  $\gamma_1 = L_1/L_0$  and  $\eta_1 = t_1/t_0$ . Here,  $L_0$  and  $t_0$  denote the length and wall thickness of the underlying large hexagons, and  $L_1$  and  $t_1$  denote the length and wall thickness of the introduced smaller hexagons, respectively. The replacement can be continued to any order of hierarchy,  $n$ , as long as the inserted hexagons are not so large that they intersect each other or previously created lower order hexagons (i.e.  $(\sum_{i=1}^n \gamma_i) \leq 0.5$  and  $(\sum_{i=j+1}^n \gamma_i) \leq \gamma_j$ ,  $0 < j < n$  and  $\gamma_i \leq \gamma_j$ ,  $i < j$ ).

In much of this paper, we have limited our study to the plastic collapse strength of first-order hierarchical honeycombs. Therefore, for the sake of simplicity, the geometrical parameters of a first-order hierarchical honeycomb are named  $\gamma$  ( $= \gamma_1$ ) and  $\eta$  ( $= \eta_1$ ). The relative density (or area fraction) of such honeycombs can be calculated as

$$\frac{\rho}{\rho_s} = \frac{2}{\sqrt{3}} \times \frac{t_0}{L_0} \times (1 + 2\gamma(2\eta - 1)) \quad (2.1)$$

where  $\rho$  is the average density of the cellular structure and  $\rho_s$  is the wall material density. The proportions of the wall material distributed in larger and smaller hexagons are equal to  $(1 - 2\gamma)/(1 - 2\gamma + 4\gamma\eta)$  and  $4\gamma\eta/(1 - 2\gamma + 4\gamma\eta)$ , respectively. For a first-order hierarchical honeycomb with  $\eta = 1$  and  $\gamma = 0.3$ , 75 per cent of the mass of the structure is allocated to the smaller honeycombs and only 25 per cent is in the remaining parts of the original hexagon.

Figure 2*a* shows a unit cell (circled) of the first-order hierarchical honeycomb, which is used for plastic analysis of the infinite structure. In-plane biaxial loading is applied in the principal structural directions  $x$  (parallel to a hexagon side) and  $y$  (perpendicular to a hexagon side). This symmetrical loading allows us to consider just half of the unit cell for elastic and plastic analyses. Owing to reflection symmetry about the  $x$ -axis of both loading and geometry, horizontal beams are moment-free. Figure 2*b* shows the free body diagram of the unit cell, where external forces  $F$  at an angle  $\theta$  from the vertical are applied to the tips of the two oblique beams with thickness  $t_0$ , and the reaction force  $2F \sin(\theta)$  is applied to the horizontal beam. Owing to the  $180^\circ$  rotational symmetry of adjacent unit cells sharing an oblique member, those oblique-beam tips (midpoints of the underlying hexagon edges) are also moment-free (see [32] for further discussion). Because force  $F$  is applied to vertical and horizontal unit cell projected areas  $\sqrt{3}L/2$  and  $3L/2$ , respectively, macroscopic normal stresses in the  $x$ - and  $y$ -directions, denoted by  $S^x$  and  $S^y$ , respectively, can be obtained from

$$F \times \sin(\theta) = S^x \times \frac{\sqrt{3}L}{2} \text{ and } F \times \cos(\theta) = S^y \times \frac{3L}{2} \quad (2.2)$$

The angle,  $\theta$ , of force  $F$  exerted on point 4 of the unit cell can be found from  $\cot(\theta) = \sqrt{3}S^y/S^x$ , and thus parametrizes all loading directions in a biaxial stress space.

### 3. Plastic collapse of the first-order hierarchical honeycomb: analytical modelling

The plastic collapse strength of the first-order hierarchical honeycomb was evaluated by classical plastic limit analysis. At the collapse load (or limit load) of a structure, plastic deformation can increase indefinitely under a constant load. This behaviour presumes that the material exhibits rigid-perfectly plastic behaviour with its associated flow rule. For our application, we took the moment versus bend angle at a plastic hinge to be a fixed ‘plastic limit moment’ (extensional yielding is discounted). It is also assumed that the loaded structure undergoes small enough displacements that the slope change of structural elements can be neglected in equilibrium calculations. This theory gives no prediction as to whether the actual nonlinear load–displacement curve is concave or convex.

We first describe a ‘lower-bound’ plastic collapse analysis of the hierarchical honeycombs. The lower bound is based on finding an equilibrium distribution of moments at or below the collapse moment, which balances the applied load. For this, we use the elastic moment distribution of a unit cell, as outlined in §3*a*. The ‘upper-bound’ plastic collapse stress is estimated analytically in §3*b*. This is based on finding the minimum collapse load (as determined by virtual work) among various mechanisms of structural deformation involving different possible locations of the plastic hinges. In our analyses, out-of-plane loads are ignored.

#### (a) ‘Lower-bound’ plastic collapse analysis

In a frame structure consisting of loaded beams, if bending moments in equilibrium with external loads are less than or equal to the plastic hinge moment of each beam cross section, then the structure either will not collapse or will be just at the point of collapse under those external loads [38]. The plastic hinge moment per unit depth of a beam with a rectangular section of thickness  $h$  and yield stress  $\sigma_{ys}$  is equal to  $\sigma_{ys}h^2/4$  (where the nonlinear contribution of axial force to collapse moment has been neglected). For our lower-bound limit analysis, we used the distribution of bending moments found via elastic analysis. The lower-bound collapse load was taken as the load sufficient to bring the calculated elastic moment in at least one cross section up to the plastic hinge moment of that cross section. Because the hierarchical structure is not statically determinate, the need for compatibility affects the actual collapse strength. While compatibility is maintained in the purely elastic regime, just one plastic hinge may not permit ongoing plastic deformation. Therefore, in general, this lower bound based on elastic analysis is expected not to quite reach the true collapse strength.

The elastic analysis used to determine the elastic moment distribution in the first-order hierarchical honeycomb under biaxial loading is an extension of that presented in Ajdari *et al.* [32] for uniaxial loading with uniform thickness,  $\eta = 1$ . The description here is abbreviated for reasons of space. Consider the free body diagram of the upper half of a structural unit cell as shown in figure 3*a*. Owing to symmetry about the  $x$ -axis, only the upper half of the unit cell was modelled, with loading by force  $F$  at angle  $\theta$ . The rotation and vertical displacement of nodes 1–3 are zero because of symmetry. The reaction forces and moments acting on nodes 1 and 2 are denoted by  $N_1$ ,  $N_2$ ,  $M_1$  and  $M_2$ . By applying force and moment balance laws to the subassembly,  $N_2$  and  $M_2$  can be written as linear functions of  $N_1$ ,  $M_1$  and  $F$ . Therefore, the bending energy stored in the subassembly can be expressed as a sum over all the beams:  $U(F, M_1, N_1) = \sum \int (M^2/(2E_s I)) ds$ , where  $M$  is the bending moment at location  $s$  along the beam,  $E_s$  is the local elastic modulus of the cell wall material and  $I$  is the beam’s cross-section moment of inertia at location  $s$  (cell walls



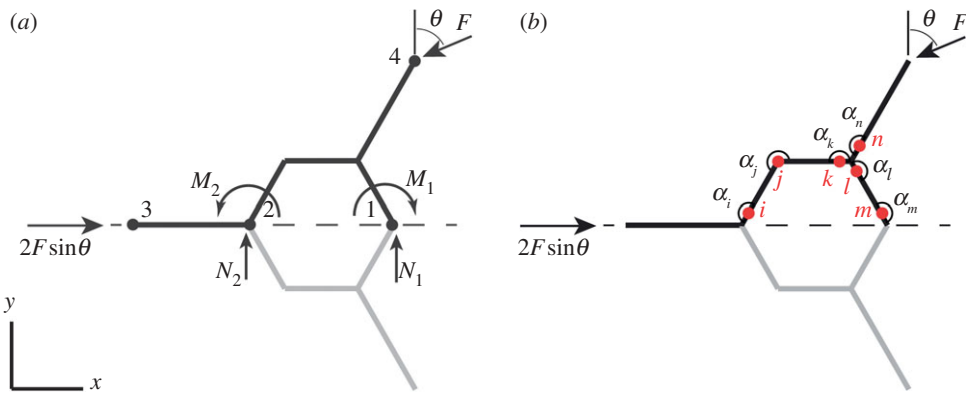


**Figure 3.** (a) Elastic reaction forces and moments exerted on the upper half of unit cell for elastic and lower-band plastic limit analyses. (b) Locations of potential plastic hinges in the upper half of unit cell for upper-band plastic limit analysis. (Online version in colour.)

are considered to have rectangular cross section with thickness,  $t$  and unit depth; i.e.  $I = t^3/12$ ). The horizontal beam connecting nodes 2 and 3 can be excluded from the energy sum because it is moment-free.

Using Castigliano's method to set the displacement and rotation of point 1 to 0 (i.e.  $\partial U/\partial N_1 = 0$ , and  $\partial U/\partial M_1 = 0$ ), one can obtain the values of reaction forces and moments at point 1,  $N_1$  and  $M_1$ , in terms of applied force,  $F$ :

$$\begin{aligned} N_1 &= F \sin(\theta)(0.231 - 0.260/\gamma) + F \cos(\theta)(0.533 + 0.150/\gamma) \\ M_1 &= F\alpha \sin(\theta)(0.029 - 0.202\gamma) + Fa \cos(\theta)(0.283\gamma - 0.017) \end{aligned} \quad (3.1)$$

These results permit the calculation of elastic moments at all potential plastic hinge locations (i.e. beam ends) in the unit cell; for any given value of  $\theta$ , the location and magnitude of the greatest moment can be determined as a function of  $F$ , and thus the lower-bound plastic strength can be described as a point in  $S_x, S_y$  space. Some lower-bound results may be seen in figure 5.

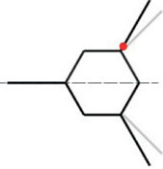
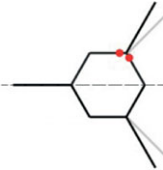
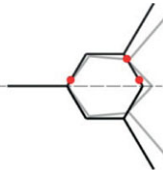
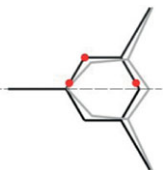
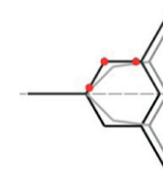
## (b) 'Upper-bound' plastic collapse analysis

According to the upper-bound theorem of plastic limit analysis for frame structures, the structure must collapse if there is a compatible pattern of plastic deformation for which the rate of work carried out by the external forces equals or exceeds the rate of internal dissipation [38]. Setting boundary work equal to internal dissipation (by the virtual work principle) permits a calculation of the necessary boundary load magnitude.

In the case of a structure with straight beams connected and loaded only at their ends (guaranteeing that the maximum bending moment occurs only adjacent to a joint), all compatible deformations of interest involve plastic hinges located where beams join nodes that make the structure a mechanism. Then, the upper-bound approach for finding collapse strength is based on comparing different mechanisms compatible with the given boundary displacements, and finding the mechanism or combination of mechanisms that minimizes the required load.

The amount of plastic energy dissipation at each hinge is given by  $M_{\text{ph}} \times |d\alpha|$ , where  $d\alpha$  is the change in angle across the plastic hinge, and  $M_{\text{ph}}$  is the positive plastic hinge (limit) moment of the cross section. A statement of virtual work for the plastically deforming structure is  $W_E(F) = \sum M_{\text{ph}}^i |d\alpha_i|$ , where  $W_E(F)$  is the work of external forces and the sum includes dissipation at all plastic hinges. While our lower-bound calculations are expected to underestimate the collapse strength, the upper-bound calculations are likely to be exact. (Because straight-beam structures develop their hinges only adjacent to the finite number of joints, if all possible end-hinged deformations are considered, the actual global minimum of the required load will be found.)

**Table 1.** Dominant deformation modes for the plastic collapse of first-order hierarchical honeycombs under uniaxial loading in  $x$ - and  $y$ -directions. The corresponding plastic collapse loads in terms of geometrical parameters  $\gamma$  and  $\eta$  are also given for each mode.

Primary basis mechanism	
I	 $\left  \frac{S_c^x}{\sigma_{ys}} \right  = \frac{1}{4 \left  1 - \frac{\cot \theta}{\sqrt{3}} \right  (1 + 2\gamma(2\eta - 1))^2 (0.5 - \gamma)} \left( \frac{\rho}{\rho_s} \right)^2$ $S_c^y = \frac{\cot \theta}{\sqrt{3}} S_c^x$
II	 $\left  \frac{S_c^x}{\sigma_{ys}} \right  = \frac{\eta^2}{2 \left  1 - \frac{\cot \theta}{\sqrt{3}} \right  (1 + 2\gamma(2\eta - 1))^2 (0.5 - \gamma)} \left( \frac{\rho}{\rho_s} \right)^2$ $S_c^y = \frac{\cot \theta}{\sqrt{3}} S_c^x$
III	 $\left  \frac{S_c^x}{\sigma_{ys}} \right  = \frac{3\eta^2}{ \sqrt{3} \cot \theta (0.25 + \gamma) - 0.75  (1 + 2\gamma(2\eta - 1))^2} \left( \frac{\rho}{\rho_s} \right)^2$ $S_c^y = \frac{\cot \theta}{\sqrt{3}} S_c^x$
IV	 $\left  \frac{S_c^x}{\sigma_{ys}} \right  = \frac{3\eta^2}{ \sqrt{3} \cot \theta (0.25 - \gamma) + 6\gamma - 0.75  (1 + 2\gamma(2\eta - 1))^2} \left( \frac{\rho}{\rho_s} \right)^2$ $S_c^y = \frac{\cot \theta}{\sqrt{3}} S_c^x$
V	 $\left  \frac{S_c^x}{\sigma_{ys}} \right  = \frac{3\eta^2}{4\gamma(1 + 2\gamma(2\eta - 1))^2} \left( \frac{\rho}{\rho_s} \right)^2$ $S_c^y = \frac{\cot \theta}{\sqrt{3}} S_c^x$
V $\propto$ 4II - III + 3IV	

Six plastic hinge locations are possible for the upper-half unit cell of a first-order hierarchical honeycomb. As shown in figure 3*b*, plastic hinges  $i, j, k, l, m$  are at the beam ends of the small hexagon with thickness  $t_1$ , and the plastic hinge  $n$  is at the lower end of the oblique beam with thickness  $t_0$ . Examining subsets of these six hinges, a total of nine plastic deformation mechanisms having just a single degree of freedom were identified for the half-cell, as given in tables 1 and 2. The deformed shape and plastic hinges for each mechanism are shown by grey lines and bullets, respectively. As shown later, mechanisms presented in table 1 are the actual deformation modes under uniaxial loading in the  $x$ - or  $y$ -direction for all values of  $\gamma, \eta$ . The mechanisms presented in table 2 are observed under various biaxial loading states oriented along  $x, y$  (i.e.  $S_c^y/S_c^x \neq 0$  or  $\infty$ ).

Note that of nine plastic hinge mechanisms presented in tables 1 and 2, there are only four *independent* deformation mechanisms, as explained below. The angular deformations at the six possible hinges (i.e. increments of the six relative angles  $\alpha_i, \alpha_j, \alpha_k, \alpha_l, \alpha_m, \alpha_n$ , in figure 3*b*) form a vector space. These deformation angles are not independent, because the five involved in the closed circuit hexagon are subject to requirements of symmetry (i.e. zero vertical displacement



**Table 2.** Dominant deformation modes for plastic collapse of first-order hierarchical honeycombs under biaxial loading in  $x$ - and  $y$ -directions. The corresponding plastic collapse loads in terms of geometrical parameters  $\gamma$  and  $\eta$  are also given for each mode.

VI		$\left  \frac{S_c^x}{\sigma_{ys}} \right  = \frac{9\eta^2}{8 \sqrt{3} \cot \theta (0.25 - \gamma) + \frac{3\gamma}{2} - 0.75 (1 + 2\gamma(2\eta - 1))^2} \left( \frac{\rho}{\rho_s} \right)^2$ $S_c^y = \frac{\cot \theta}{\sqrt{3}} S_c^x$
	VI $\propto$ 12II - 3III + IV	
VII		$\left  \frac{S_c^x}{\sigma_{ys}} \right  = \frac{\eta^2}{ \sqrt{3} \cot \theta (0.25 - \gamma) + 2\gamma - 0.75 (1 + 2\gamma(2\eta - 1))^2} \left( \frac{\rho}{\rho_s} \right)^2$ $S_c^y = \frac{\cot \theta}{\sqrt{3}} S_c^x$
	VII $\propto$ -4II + III	
VIII		$\left  \frac{S_c^x}{\sigma_{ys}} \right  = \frac{9\eta^2}{4 \sqrt{3} \cot \theta (0.25 + \frac{\gamma}{2}) + \frac{3\gamma}{2} - 0.75 (1 + 2\gamma(2\eta - 1))^2} \left( \frac{\rho}{\rho_s} \right)^2$ $S_c^y = \frac{\cot \theta}{\sqrt{3}} S_c^x$
	VIII $\propto$ 3II - III	
IX		$\left  \frac{S_c^x}{\sigma_{ys}} \right  = \frac{9\eta^2}{4 \sqrt{3} \cot \theta (0.25 - \frac{\gamma}{2}) + \frac{9\gamma}{2} - 0.75 (1 + 2\gamma(2\eta - 1))^2} \left( \frac{\rho}{\rho_s} \right)^2$ $S_c^y = \frac{\cot \theta}{\sqrt{3}} S_c^x$
	IX $\propto$ -III + 3IV	

and rotation of node 1 lying on the line of symmetry). The changes in angles  $\alpha_i$  to  $\alpha_n$ , therefore, satisfy

$$\begin{aligned} d\alpha_i + d\alpha_j + d\alpha_k + d\alpha_l + d\alpha_m &= 0 \quad (\text{sum of angles in a loop}) \\ 4d\alpha_i + 3d\alpha_j + d\alpha_k + d\alpha_l &= 0 \quad (\text{vertical displacement of node 1}). \end{aligned} \quad (3.2)$$

Therefore, for the five variables  $d\alpha_i$  to  $d\alpha_m$ , only three can be chosen independently. (Note that mechanism I is uniquely independent because it alone involves hinge  $n$ .) For mechanisms I–V, the changes in angle at plastic hinges  $i - n$ , represented in the form  $[d\alpha_i, d\alpha_j, d\alpha_k, d\alpha_l, d\alpha_m, d\alpha_n]$ , are proportional to  $[0,0,0,0,0,1]$ ,  $[0,0,1,-1,0,0]$ ,  $[1,0,0,-4,3,0]$ ,  $[3,-4,0,0,1,0]$  and  $[2,-3,1,0,0,0]$ , respectively. Deformed configurations illustrating mechanisms I–IV are shown in figure 4. We have selected I–IV as a convenient primary basis for all deformations, and tables 1 and 2 describe each additional mechanism in terms of these.

The single degree of freedom mechanisms VI–IX shown in table 2 minimize load only under some non-uniaxial loadings only (i.e.  $S_c^y, S_c^x \neq 0$ ). The change in angle at plastic hinges  $i - n$  for these mechanisms is proportional to  $[0,1,-3,0,2,0]$ ,  $[1,0,-4,0,3,0]$ ,  $[0,1,0,-3,2,0]$ ,  $[2,-3,0,1,0,0]$ , respectively.

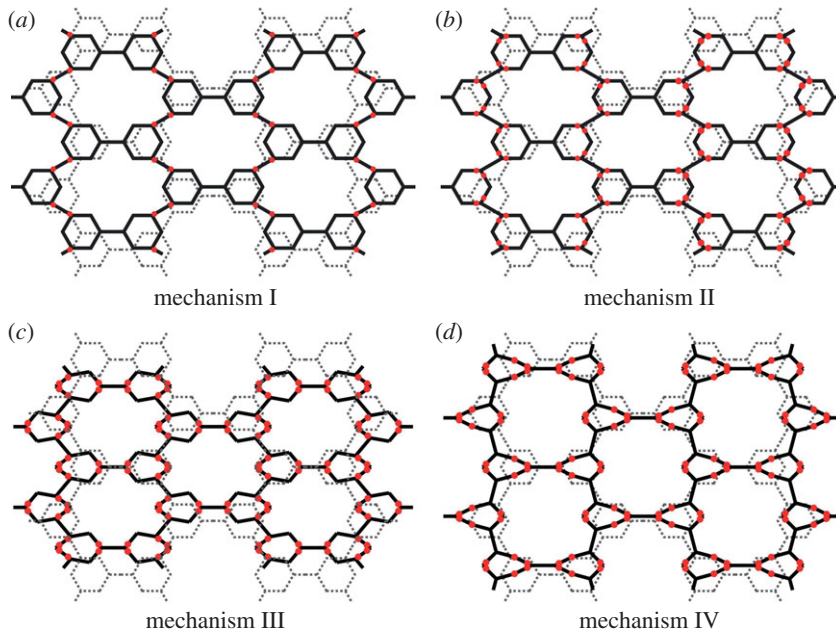


**Figure 4.** (a–d) Deformed configurations of plastic collapse for hierarchical honeycomb according to the mechanisms I–IV, involving different plastic hinge locations marked by bullets. (Online version in colour.)

Algebraic expressions for the normalized  $x$ -direction plastic collapse stress corresponding to each mechanism are also presented in tables 1 and 2. These are derived as follows: parametrizing each mechanism in terms of the plastic hinge angular deformation vector  $[d\alpha_i, d\alpha_j, d\alpha_k, d\alpha_l, d\alpha_m, d\alpha_n]$  one can express the  $x, y$  displacements of node 4 with respect to node 3 as

$$dx = - \left[ \frac{\sqrt{3}}{4}, \frac{\sqrt{3}(0.5 - \gamma)}{2}, \frac{\sqrt{3}(0.5 - \gamma)}{2}, \frac{\sqrt{3}(0.5 - \gamma)}{2} \right] L_o \cdot [d\alpha_i, d\alpha_j, d\alpha_k, d\alpha_n] \quad (3.3)$$

$$dy = \left[ \left( \frac{1}{4} + \gamma \right), \left( \frac{1}{4} + \frac{\gamma}{2} \right), \left( \frac{1}{4} - \frac{\gamma}{2} \right), \left( \frac{1}{4} - \frac{\gamma}{2} \right) \right] L_o \cdot [d\alpha_i, d\alpha_j, d\alpha_k, d\alpha_n].$$

Then, the work of force  $F$  at angle  $\theta$  is represented as  $W(F) = -F \sin \theta dx - F \cos \theta dy$ . Plastic dissipation can be expressed as

$$PD = \sigma_{ys} \frac{t_1^2}{4} \times (|d\alpha_i| + |d\alpha_j| + |d\alpha_k| + |d\alpha_l| + |d\alpha_m|) + \sigma_{ys} \frac{t_0^2}{4} \times |d\alpha_n| \quad (3.4)$$

Setting equal the expression of internal dissipation and external work, the critical force per unit depth,  $F_c$ , required to deform each mechanism can be given as a function of  $\theta$ .

For example, for mechanism I, parametrized as  $[0, 0, 0, 0, 0, 1]$ , the required force is obtained as

$$F_c = \frac{\sigma_{ys} t_0^2 / 4}{L_o |\sin(\theta - \pi/6)|(0.5 - \gamma)} \quad (3.5)$$

By substituting the expression for density (equation (2.1)) and the relationship between applied biaxial stresses and load (equation (2.2)), the components of stress activating this mechanism are found in terms of  $\theta$  as

$$\left| \frac{S_c^x}{\sigma_{ys}} \right| = \frac{1}{4 \left| \left( 1 - \frac{\cot \theta}{\sqrt{3}} \right) \right| (1 + 2\gamma(2\eta - 1))^2 (0.5 - \gamma)} \left( \frac{\rho}{\rho_s} \right)^2 \quad (3.6)$$

$$S_c^y = \frac{\cot \theta}{\sqrt{3}} S_c^x$$

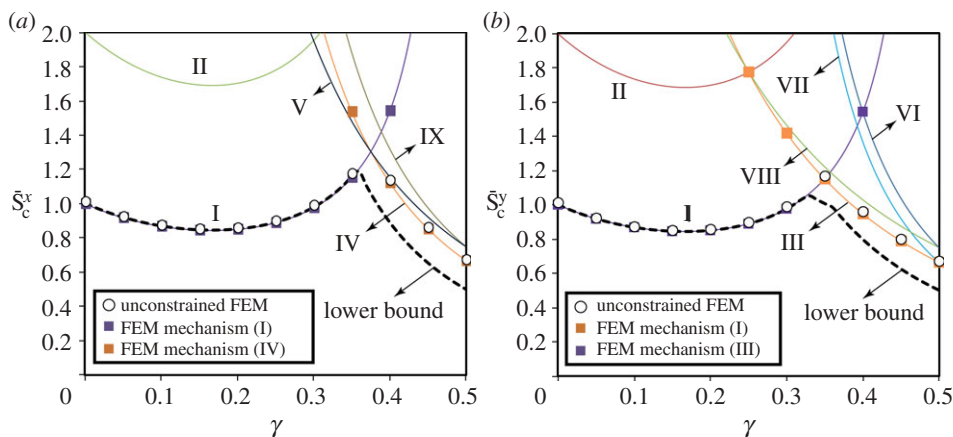


**Figure 5.** Normalized plastic collapse strength of uniform thickness hierarchical honeycomb under uniaxial loading in (a)  $x$ - and (b)  $y$ -directions as a function of length ratio,  $\gamma$ . The plastic collapse load is normalized by that of a regular honeycomb of the same density. The actual strength is on the curves marked by circles (where least upper bound happens to match unconstrained finite-element analysis). (Online version in colour.)

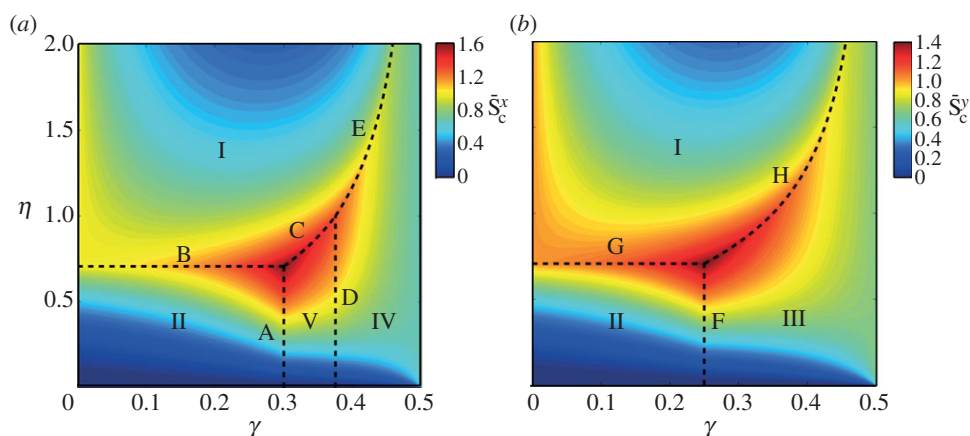


**Figure 6.** Normalized plastic collapse strength for the first-order hierarchical honeycomb under uniaxial loading in (a)  $x$ - and (b)  $y$ -directions, as determined analytically from upper-bound analysis. Strength is normalized by that of a regular honeycomb of the same density and plotted as a function of length ratio,  $\gamma$ , and thickness ratio,  $\eta$ . The numbered areas correspond to different (least) upper-bound mechanisms from table 1. (Online version in colour.)

These expressions are entered into the first row of table 1. Mechanism I is the well-known simple mechanism involved in the plastic collapse of a regular honeycomb structure [39].

Note that plastic collapse strength is proportional to the square of the relative density, which is consistent with the classical relationships for strength of bending-dominated cellular structures [39]. By numerically or algebraically finding the lowest calculated upper-bound strength, it is possible to determine which mechanism controls the collapse behaviour for any specific structural parameters and loading. Over the entire admissible range of  $\eta > 0$ ,  $0 \leq \gamma \leq 0.5$ , mechanisms I–VIII yield the minimum collapse load at certain loading/geometry combinations, and therefore are the dominant mechanisms over certain ranges of  $\eta$ ,  $\gamma$ . (Mechanism IX never yields the minimum collapse load and thus is not dominant under any biaxial loading or honeycomb geometry.) Under uniaxial loading in the  $x$ -direction, only four mechanisms, I, II, IV and V are potentially dominant over the entire admissible range of  $\eta$  and  $\gamma$  (figures 5 and 6). Similarly, for uniaxial loading in the  $y$ -direction, the three potentially dominant mechanisms are I, II and III.

## 4. Plastic collapse analysis: numerical simulations

Finite-element simulations were carried out to confirm the analytical upper-bound results of the previous section. A unit cell of the structure was modelled and meshed (100 elements per beam) using elastic—perfectly plastic two-node cubic beam elements (B23) in ABAQUS. Two kinds of study were performed: (i) pre-selecting locations for plastic hinges according to each specific deformation mechanism, thereby evaluating its associated collapse load; (ii) simulating plastic collapse of the structure with plastic hinge locations unspecified, and finding a plateau in the load. We limited these simulations to uniaxial loading in either  $x$ - or  $y$ -directions. The unit cell was subjected to displacement-controlled compression in the direction of loading, with free expansion in the transverse direction. Strength was defined as the stress associated with the level plateau in the force–displacement curve. In the finite-element results presented in this paper, the elastic modulus and Poisson’s ratio were taken as  $E_s = 200$  GPa and  $\nu = 0.3$ , respectively.

### (a) Finite-element simulation of individual plastic collapse mechanisms

To model each individual plastic collapse mechanism, we permitted plastic behaviour only at certain hinges specified for that mechanism. To achieve this, individual elements at the desired hinge locations (just the first or last of 100 elements along that beam) were given elastic–perfectly plastic bending relations, whereas the remaining elements of that beam were specified as linear elastic with the same modulus. This permitted direct comparison with the upper-bound analytical result for that mechanism.

### (b) Finite-element simulation of the general plastic collapse

Finite-element analysis (FEA) was also used to compute the deformation without mode pre-selection. The simulations were analogous to the simulations described in the previous section except that elastic/perfectly plastic bending behaviour was assigned to all elements, so hinge locations could be found by the finite-element computations.

## 5. Results: plastic collapse of first-order hierarchical honeycombs

Here, the analytical and numerical results for plastic collapse strength of the first-order hierarchical honeycomb under uniaxial (§5*a*) and biaxial loading (§5*b*) are presented. The trade-off between stiffness and plastic collapse by introducing of the first level of hierarchy is discussed in §5*c*.

### (a) Plastic collapse under uniaxial $x, y$ loading

The above-described analytical and numerical models were used to estimate the plastic collapse strength under uniaxial loading in the  $x$ - and  $y$ -directions. The values of collapse strength in each direction, after being normalized by the collapse strength of a regular honeycomb of the same density, are denoted by  $\bar{S}_c^x = S_c^x/S_c$  and  $\bar{S}_c^y = S_c^y/S_c$ , where  $S_c$  denotes the collapse strengths of a regular honeycomb. Note that both the  $x$  and  $y$  collapse strengths of a regular honeycomb equal  $S_c = 0.5\sigma_{ys}(\rho/\rho_s)^2$  [39].

The normalized uniaxial collapse strength (in both  $x$ - and  $y$ -directions) of the uniform thickness ( $\eta = 1$ ) first-order hierarchical honeycomb structure is shown as a function of  $\gamma$  in figures 5*a* and *b*, respectively. These graphs present the results of four kinds of analysis:

- the solid lines show the analytical upper-bound strengths of each named deformation mechanism shown in tables 1 and 2 (i.e. plots of the strength expression derived for each table entry);

- the square points represent constrained FEA (§4a), and fall perfectly on the solid analytical lines of the modes they represent. This agreement of manual analysis and FEA for the same plastic hinges implies that both approaches were carried out without error;
- the dashed line shows the analytical lower-bound strength based on an elastic moment distribution. It is nowhere above the solid upper-bound curve. Over the range of  $0 \leq \gamma < 0.36$  for  $x$  loading, and  $0 \leq \gamma < 0.32$  for  $y$  loading, it falls exactly on the upper-bound curve for deformation mode I—such equality of upper- and lower-bound calculations implies an ‘exact’ calculation of strength. But relative to deformation modes III and VII, the lower-bound result is well below the upper-bound result. As explained earlier, we anticipate that when lower- and upper-bound disagree, the upper bound is more likely correct; and
- circular points represent ‘unconstrained’ finite-element results from simulating the actual structural response (§4b). It may be observed that these numerical results fall precisely on the lowest upper-bound curves.

In summary, we take both the analytical upper-bound method (when the deformation mode with least required load for the given boundary displacement is selected), and the unconstrained FEA, as providing equally accurate collapse strength estimations.

These results show that when  $\eta = 1$ , the structure fails according to deformation mode I over the range  $0 \leq \gamma < 0.375$  for  $x$  loading and  $0 \leq \gamma < 0.35$  for  $y$  loading. For greater  $\gamma$  values, mode IV is controlling for uniaxial loading in the  $x$ -direction, and III for uniaxial loading in the  $y$ -direction. Note that the values of collapse strength according to some of the mechanisms in tables 1 and 2 are too great to appear in the figures as currently scaled. That is because the collapse strengths according to mechanisms I and II approach infinity as  $\gamma$  approaches 0.5, because, in each case, the displacement of the point on which the external force  $F$  acts (figure 3b) approaches zero in the relevant (horizontal or vertical) direction. For any mechanism, the computed strength may approach infinity if some value of  $\gamma$  can make the denominator vanish. Compared with regular honeycombs, the plastic collapse strength of the first-order hierarchical honeycomb of uniform thickness shows a maximum-normalized value of 1.3 and 1.15 in uniaxial loading in  $x$ - and  $y$ -directions, occurring at  $\gamma = 0.375$  and  $\gamma = 0.35$ , respectively. Also, the plastic collapse strength reaches the minimum value of two-thirds at  $\gamma = 0.375$  driven by mechanism III.

Figure 6 introduces the effects of thickness-ratio variation (i.e. varying  $\eta$ ) on uniaxial  $x$  and  $y$  strength, as calculated by upper-bound analysis. The plots represent the lower envelope of strength for the previously defined mechanisms, for thickness ratios  $0 < \eta \leq 2$ , and length ratios  $0 \leq \gamma \leq 0.5$ . The strength is again normalized by that of a regular honeycomb with the same density. Under uniaxial loading in the  $x$ -direction (figure 6a), the four mechanisms I, II, IV and V are the dominant mechanisms over the entire admissible range of  $\eta$  and  $\gamma$ —this was observed by plotting the upper-bound strength expressions in the finite domain, and then was proved by algebraic comparison of the derived strength expressions. The five boundary segments denoted by A, B, C, D and E bordering the five regions are found by equating the strength expressions of adjoining deformation modes to give:

$$\begin{aligned}
 \text{A: } \gamma &= \frac{3}{10} & 0 < \eta < \frac{1}{\sqrt{2}} \\
 \text{B: } \eta &= 1/\sqrt{2} & 0 < \gamma < 3/10 \\
 \text{C: } \eta &= \left(\frac{2\gamma}{3-6\gamma}\right)^{0.5} & \frac{3}{10} < \gamma < \frac{3}{8} \\
 \text{D: } \gamma &= \frac{3}{8} & 0 < \eta < 1 \\
 \text{E: } \eta &= \left(\frac{8\gamma-1}{8-16\gamma}\right)^{0.5} & \frac{5}{16} < \gamma < 0.5.
 \end{aligned}$$

The maximum-normalized plastic collapse load,  $\bar{S}_c^x = 1.6$ , occurs at the optimal values of  $\gamma = 0.3$  and  $\eta = 1/\sqrt{2} \approx 0.71$ , where curves A, B and C join. Along the  $\eta = 0.71$  line, the normalized plastic collapse load of structure is greater than 1 over a relatively wide range of  $\gamma$  ( $0 < \gamma < 0.4$ ). This contrasts with the uniform thickness structure (figure 5a) where for  $0 < \gamma < 0.3$  and  $0.42 < \gamma < 0.5$  the collapse load of the structure is below 1.

For  $y$  direction uniaxial loading (figure 6b), the dominant mechanisms of plastic collapse are I, II and III. The relationships defining the three border lines of the dominant mechanisms, as denoted by F, G and H, can be derived as:

$$\begin{aligned} \text{F: } \gamma &= 0.25 & 0 < \eta < \frac{1}{\sqrt{2}} \\ \text{G: } \eta &= \frac{1}{\sqrt{2}} & 0 < \gamma < 0.25 \\ \text{H: } \eta &= \left( \frac{4\gamma + 1}{-16\gamma + 8} \right)^{1/2} & 0.25 < \gamma < 0.5 \end{aligned}$$

The maximum-normalized plastic collapse load,  $\bar{S}_c^y = 1.37$ , occurs at the optimal values of  $\gamma = 0.25$  and  $\eta = 0.71$  at the meeting point of curves F–H.

Along the  $\eta = 0.71$  line, the normalized  $y$ -direction plastic collapse strength exceeds 1 for honeycombs with  $0 < \gamma < 0.35$ , compared with the uniform thickness structure (i.e.  $\eta = 1$ ) where in the range of  $0 < \gamma < 0.3$  and  $0.39 < \gamma < 0.5$ , the normalized plastic collapse strength of the structure is less than 1.

These  $x, y$  strength results show that the collapse behaviour of the hierarchical honeycomb can be improved by introducing different thickness ratios (i.e. departing from  $\eta = 1$ ). The collapse strength of hierarchical honeycombs with thickness variation in the  $x$  and  $y$  directions can be increased by almost 23 and 22 per cent, respectively, compared with the hierarchical honeycomb of uniform thickness.

## (b) Plastic collapse surface under biaxial $x, y$ loading

The foregoing collapse strength results were for uniaxial stress in either the  $x$ - or  $y$ -direction. However, our analytical upper-bound calculations (which we take to be exact) also encompass simultaneous application of differing  $\bar{S}^x$  and  $\bar{S}^y$ . As before, the values of biaxial collapse strength in  $x$ - and  $y$ -directions are normalized by the  $x$  and  $y$  uniaxial collapse strength of a regular honeycomb of the same density, respectively.

For particular values of  $\gamma$  and  $\eta$ , the least of all the analytical upper-bound strengths can be plotted on a failure locus in  $\bar{S}^x, \bar{S}^y$  space. Figure 7 gives the convex normalized collapse boundary for a first-order hierarchical structure, which is found by varying  $\theta$  in the equations given in table 1, and constructing the innermost boundary of their union. Curves are given for several values of  $\gamma$  ( $0 =$  no hierarchy,  $0.25, 0.31, 0.5$ ) and two values of  $\eta$  ( $1 =$  uniform thickness and  $0.71$ ).

The plastic collapse surface of a regular honeycomb structure ( $\gamma = 0$ ) forms two parallel  $45^\circ$  lines, because only the difference in  $\bar{S}^x, \bar{S}^y$  causes bending of the beams, which are taken to have infinite axial strength. As expected, at  $\eta = 0.71$ , the plastic collapse surface is wider in all directions than the case of  $\eta = 1$ . Each facet of the plastic collapse ‘polygon’ for any given value of  $\gamma$  corresponds to a mechanism from table 1, but to minimize clutter these have not been indicated. (For example, for the first-order hierarchical honeycomb with  $\gamma = 0.25$  and  $\eta = 1$ , the mechanisms [I,VI,VIII,I,VI,VIII,I] are dominant over entire range of biaxial loading, starting from the horizontal axis intercept and continuing anticlockwise around the polygon to reach the starting point.)

Hierarchical honeycombs demonstrate a bending-dominated behaviour under any biaxial loading, not just those with  $S^X \neq S^Y$ . This is obvious from a simple geometrical argument: in a hierarchical honeycomb, every other vertex of each introduced hexagon is a junction of only two non-collinear beams, which experience bending under any direction of end loading.



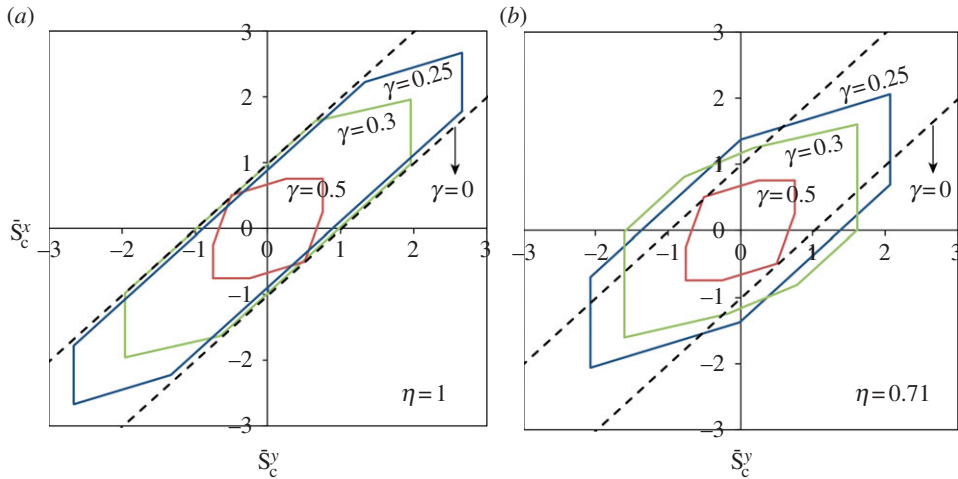


**Figure 7.** Plastic collapse surface of first-order hierarchical honeycombs under biaxial loading in horizontal and vertical directions for different values of  $\gamma$  and (a)  $\eta = 1$  and (b)  $\eta = 0.71$ . The plastic collapse load is normalized by that of a regular honeycomb of the same density. (Online version in colour.)

### (c) Stiffness-uniaxial collapse strength

Using the elastic analysis method described briefly in §3a, the effective Young's modulus was evaluated for a first-order hierarchical honeycomb including thickness variation:

$$\frac{E}{E_s} \left/ \left( \frac{t_o}{L_o} \right)^3 \right. = \frac{(40\sqrt{3})\eta^3}{(30 - 180\gamma + 360\gamma^2 - 240\gamma^3)\eta^3 + 39\gamma - 216\gamma^2 + 356\gamma^3}, \quad (5.1)$$

for a first-order hierarchical honeycomb with uniform wall thickness,  $\eta = 1$ , this yields,

$$\frac{E}{E_s} \left/ \left( \frac{t_o}{L_o} \right)^3 \right. = \frac{\sqrt{3}}{0.75 - 3.525\gamma + 3.6\gamma^2 + 2.9\gamma^3}. \quad (5.2)$$

In figure 8, we have plotted the analytically determined (upper-bound calculation) normalized plastic collapse strength versus the normalized Young's modulus for honeycombs with varying thickness ratio parameter,  $\eta$ . Plastic collapse strength and stiffness were normalized by the plastic collapse strength and stiffness of a regular honeycomb of the same density. The plots are formed by superposing a large number of space curves with coordinates  $\bar{E}$  and  $\bar{S}_c^x$  or  $\bar{S}_c^y$ , each representing a different value of  $\eta$  while  $\gamma$  is varied over its entire feasible range ( $0 \leq \gamma \leq 0.5$ ). Figure 8a shows the  $\bar{E}$ ,  $\bar{S}_c^x$  view, whereas figure 8b shows the  $\bar{E}$ ,  $\bar{S}_c^y$  view. Note that when  $\gamma$  reaches its limits, there is no influence of  $\eta$ , so all the different space curves emerge from points representing  $\gamma = 0$  and 0.5. As is seen most clearly for figure 8b, the curve for  $\eta = 1$  emerges from  $\gamma = 0$ , switches to a different mode at  $\gamma = 0.35$ , and ends at  $\gamma = 0.5$ .

The highest achievable value of normalized stiffness (observable in both figures) is 2.15, obtained at  $\gamma \cong 0.30$  and  $\eta = 0.76$ . At that point the  $x$  and  $y$  normalized strengths are 1.46 and 1.21, respectively. The greatest normalized uniaxial  $x$ -direction strength is 1.60, at that point the normalized stiffness is 2.14, and the  $y$  normalized strength is 1.17. By contrast, the greatest normalized  $y$  strength is 1.37, and at that point the normalized stiffness is 1.93 and the  $x$  strength is 1.37. Therefore, if we ask for equal  $x$  and  $y$  strength, the greatest normalized value seems to be 1.37, where normalized stiffness is 1.93. The presented graphs show that a wide range of in-plane uniaxial stiffness and uniaxial collapse strength values can be obtained for first-order hierarchical honeycombs by varying the geometrical parameters,  $\gamma$  and  $\eta$ .

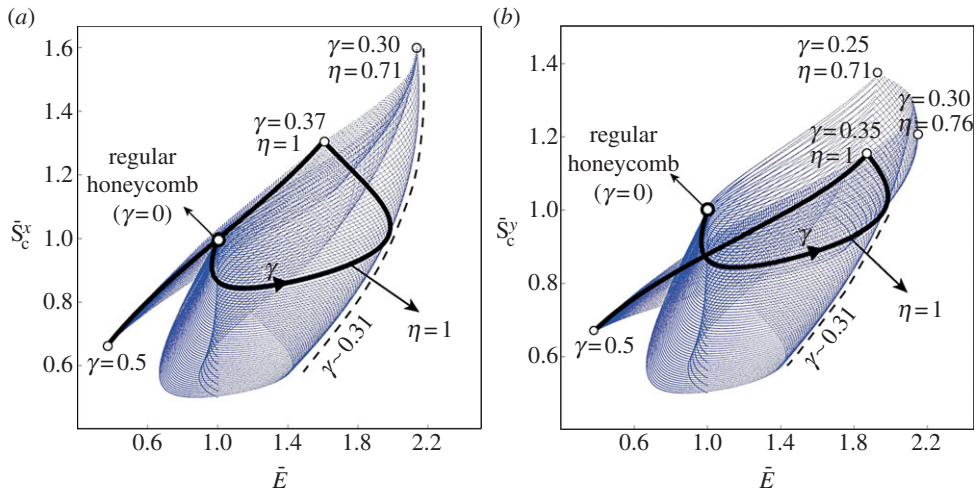


**Figure 8.** Plastic collapse strength versus stiffness of first-order hierarchical honeycombs under uniaxial loading in (a)  $x$ - and (b)  $y$ -directions, respectively. The plastic collapse strength and stiffness are normalized by those of a regular honeycomb of the same density. (Online version in colour.)

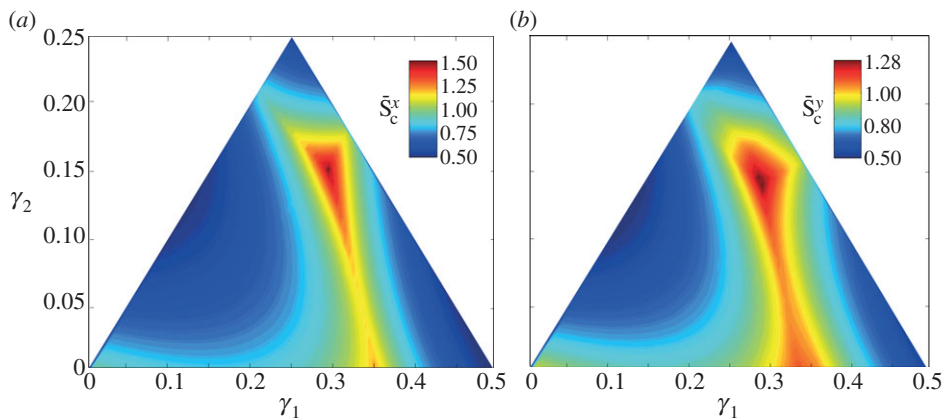


**Figure 9.** Contours of plastic collapse strength of second-order honeycombs of uniform thickness ( $\eta = 1$ ) under uniaxial loading in (a)  $x$ - and (b)  $y$ -directions for different values  $\gamma_1$  and  $\gamma_2$ , respectively. The plastic collapse strength is normalized by that of a regular honeycomb of the same density. (Online version in colour.)

## 6. Stiffness and plastic collapse of higher-order hierarchical honeycombs

Motivated by the increasing trend in the maximum values of stiffness and collapse strength observed for first-order honeycombs in comparison with the counterpart regular honeycombs, we extended our study to higher-order honeycombs. The analytical estimation of plastic collapse strength was not practical because of the increase in the number of possible mechanisms of collapse caused by introducing additional beams for each level of hierarchy. Instead, the finite-element method explained in §4*b* was used on honeycomb unit cells to simulate the plastic collapse of honeycombs with perfectly plastic material properties. Finite-element models with varying geometries were created in MATLAB, and were solved using ABAQUS.

Figure 9*a,b* shows the normalized plastic collapse of second-order honeycombs with varying  $\gamma_1$  and  $\gamma_2$  values and uniform thickness ( $\eta_1 = \eta_2 = 1$ ) under uniaxial loading under  $x$ - and  $y$ -directions, respectively. The maximum value of normalized collapse strength is  $\bar{S}_c^x = 1.5$  and

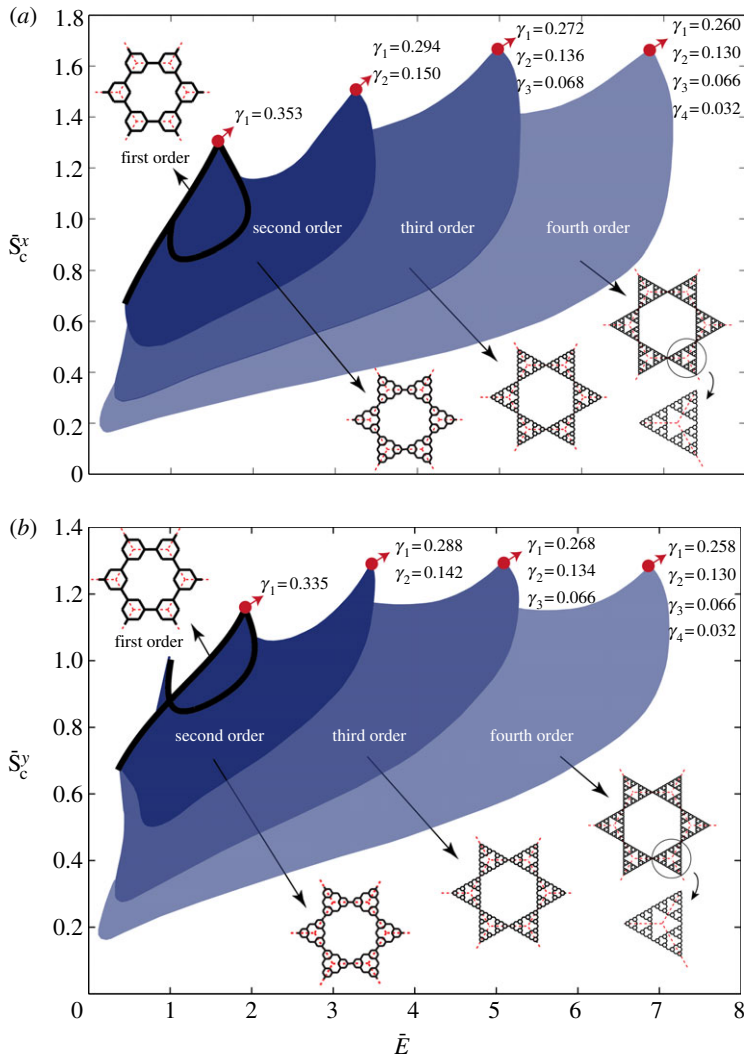


**Figure 10.** Plastic collapse strength versus stiffness for first-, second-, third- and fourth-order hierarchical honeycombs of uniform thickness ( $\eta = 1$ ) under uniaxial loading in (a)  $x$ - and (b)  $y$ -directions, respectively. The bullets specify the geometries for each order of hierarchy resulting in the maximum attainable specific strength. Plastic collapse strength and stiffness are normalized by those of a regular honeycomb of the same density. (Online version in colour.)

$\bar{S}_c^y = 1.28$  in  $x$ - and  $y$ -directions, occurring at  $(\gamma_1, \gamma_2) = (0.29, 0.15)$  and  $(\gamma_1, \gamma_2) = (0.29, 0.14)$ , respectively. The minimum value of normalized collapse strength along  $x$ - and  $y$ -directions is 0.5 which occurs at  $\gamma_1 = 0.125$  and  $\gamma_2 = 0.125$ .

Figure 10*a,b* shows maps of normalized collapse strength versus normalized stiffness for regular, first-, second-, third- and fourth-order honeycombs of uniform thickness in  $x$ - and  $y$ -directions, respectively, obtained from the FEA. It should be noted that a  $n$ th-order hierarchical honeycomb is a special configuration of honeycombs with higher order of hierarchy. For example, a second-order hierarchical honeycomb is a special configuration of third-order hierarchical honeycombs with,  $\gamma_3 = 0$ . Thus, the entire coloured area in figure 10 displays the range of achievable stiffness and strength with introducing four orders of hierarchy in the architecture of a regular honeycomb. The graphs show the large increase in the achievable range of stiffness and plastic collapse strength permitted by increasing the order of hierarchy. The enhancement in

the normalized stiffness is more notable with the maximum-normalized stiffness increasing from 2 and 3.5 for first- and second-order hierarchical honeycombs to 5.3 and 7.1 for third- and fourth-order hierarchical honeycombs. The maximum value of plastic collapse strength experiences an increase of [30, 50 and 68%] in  $x$ - and [15, 28 and 30%] in  $y$ -directions for [first, second and third] orders of hierarchy in comparison with a regular honeycomb of the same mass. Introducing the fourth order of hierarchy does not result in significant increase in the maximum-normalized strength in either loading condition.

## 7. Conclusions

A regular hexagonal honeycomb structure is iteratively modified at successively smaller length scales to create a novel class of self-similar hierarchical honeycombs. The modification consists of replacing each three-beam joint with a small hexagon, aligned parallel to the original honeycomb. By adjusting the side length and side thickness of the small replacement hexagons, a rich class of structures is created. First and second iterations of such hierarchical honeycombs with uniform wall thickness were recently shown to provide up to two and 3.5 times the specific stiffness of the regular honeycomb of the same density [32].

To understand the multi-axial limit strength of hierarchical honeycombs and its relationship with the honeycomb architecture, first, we investigated the plastic collapse strength of first-order hierarchical honeycombs using upper-bound analytical models. Finite-element simulations were also carried out to validate the proposed analytical models. Depending on the substitution ratios for length and thickness, the resulting structure can exhibit many possible stiffness-strength properties relative to regular honeycombs of the same density, including (stiffer/stronger), (stiffer/weaker) and (more compliant/weaker) properties. The significance of these results is most evident when examining the amount of improvement, relative to the counterpart regular honeycomb of the same mass per unit area, in both uniaxial stiffness and uniaxial limit strength simultaneously.

Our study is unique in exploring (partly analytically and partly numerically) a substantial region of parameter space. This includes length and thickness substitution ratios up to fourth order of hierarchy, and the entire range of principal stress ratios. Beyond the specific improvements afforded by this particular case of hierarchical refinement, we suggest that this comprehensive study involving a truly iterative substitution scheme may serve as a useful illustration of hierarchical behaviour. The findings of this study therefore suggest new avenues for the understanding and development of novel materials and structures with desirable and perhaps actively tailorable properties.

The authors thank Professors John W. Hutchinson and Hamid Nayeb-Hashemi and Dr Amin Ajdari for many constructive comments and helpful discussions. This work was supported by the US Air Force Office of Scientific Research under AFOSR YIP grant award (no. FA 9550-10-1-0145) under the technical supervision of Dr Joycelyn Harrison.

## References

1. Gu S, Lu TJ, Evans AG. 2001 On the design of two-dimensional cellular metals for combined heat dissipation and structural load capacity. *Int. J. Heat Mass Transf.* **44**, 2163–2175. (doi:10.1016/S0017-9310(00)00234-9)
2. Lu TJ, Stone HA, Ashby MF. 1998 Heat transfer in open-cell metal foams. *Acta Mater.* **46**, 3619–3635. (doi:10.1016/S1359-6454(98)00031-7)
3. Vaziri A, Hutchinson JW. 2007 Metal sandwich plates subject to intense air shocks. *Int. J. Solids Struct.* **44**, 2021–2035. (doi:10.1016/j.ijsolstr.2006.08.038)
4. Vaziri A, Xue Z, Hutchinson J. 2006 Metal sandwich plates with polymer foam-filled cores. *J. Mech. Mater. Struct.* **1**, 97–127. (doi:10.2140/jomms.2006.1.97)
5. Vaziri A, Xue Z, Hutchinson JW. 2007 Performance and failure of metal sandwich plates subjected to shock loading. *J. Mater. Struct.* **2**, 1947–1963. (doi:10.2140/jomms.2007.2.1947)

6. Wadley HNG. 2006 Multifunctional periodic cellular metals. *Phil. Trans. R. Soc.* **364**, 31–68. (doi:10.1098/rsta.2005.1697)
7. Wadley HNG, Fleck NA, Evans AG. 2003 Fabrication and structural performance of periodic cellular metal sandwich structures. *Compos. Sci. Technol.* **63**, 2331–2343. (doi:10.1016/S0266-3538(03)00266-5)
8. Henry C, McKnight G. 2006 Cellular variable stiffness materials for ultra-large reversible deformations in reconfigurable structures. *Smart Structures and Materials 2006: Active Materials: Behaviour and Mechanics*, 617023. (doi:10.1117/12.659633)
9. Ju J, Summers JD. 2011 Compliant hexagonal periodic lattice structures having both high shear strength and high shear strain. *Mater. Des.* **32**, 512–524. (doi:10.1016/j.matdes.2010.08.029)
10. Wan H, Ohtaki H, Kotosaka S, Hu G. 2004 A study of negative Poisson's ratios in auxetic honeycombs based on a large deflection model. *Eur. J. Mech. A Solids* **23**, 95–106. (doi:10.1016/j.euromechsol.2003.10.006)
11. Jackman RJ, Brittain ST, Adams A, Prentiss MG, Whitesides GM. 1998 Design and fabrication of topologically complex, three-dimensional microstructures. *Science* **280**, 2089–2091. (doi:10.1126/science.280.5372.2089)
12. Larsen UD, Sigmund O, Bouwstra S. 1996 Design and fabrication of compliant micromechanisms and structures with negative Poisson's ratio. In *Micro Electro Mechanical Systems, 1996, MEMS'96, Proc. An Investigation of Micro Structures, Sensors, Actuators, Machines and Systems. IEEE, The Ninth Annual Int. Workshop on IEEE*, pp. 365–371.
13. Levy O, Krylov S, Goldfarb I. 2006 Design considerations for negative Poisson ratio structures under large deflection for MEMS applications. *Smart Mater. Struct.* **15**, 1459. (doi:10.1088/0964-1726/15/5/035)
14. Howell LL. 2001 *Compliant mechanisms. 21st Century kinematics*, pp. 189–216. New York, NY: John Wiley & Sons.
15. Kota S, Joo J, Li Z, Rodgers SM, Sniogowski J. 2001 Design of compliant mechanisms: applications to MEMS. *Analog Integr. Circuits Signal Process.* **29**, 7–15. (doi:10.1023/A:1011265810471)
16. Lim T-C. 2004 Elastic properties of a Poisson-shear material. *J. Mater. Sci.* **39**, 4965–4969. (doi:10.1023/B:JMSC.0000035347.69053.af)
17. Bornengo D, Scarpa F, Remillat C. 2005 Evaluation of hexagonal chiral structure for morphing airfoil concept. *Proc. Inst. Mech. Eng. G, J. Aerospace Eng.* **219**, 185–192. (doi:10.1243/095441005X30216)
18. Bubert EA, Woods BK, Lee K, Kothera CS, Wereley NM. 2010 Design and fabrication of a passive 1D morphing aircraft skin. *J. Intell. Mater. Syst. Struct.* **21**, 1699–1717. (doi:10.1177/1045389X10378777)
19. Heo H, Ju J, Kim D-M, Jeon C-S. 2011 *Passive morphing airfoil with honeycombs*. In *Proc. ASME Int. Mechanical Engineering Congress and Exposition, IMECE2011–64350, Denver, CO, USA*.
20. Johnson T, Frecker M, Abdalla M, Gurdal Z, Lindner D. 2009 Nonlinear analysis and optimization of diamond cell morphing wings. *J. Intell. Mater. Syst. Struct.* **20**, 815–824. (doi:10.1177/1045389X08098098)
21. Lesieutre G, Browne JA, Frecker M. 2011 Scaling of performance, weight, and actuation of a 2-D compliant cellular frame structure for a morphing wing. *J. Intell. Mater. Syst. Struct.* **22**, 979–986. (doi:10.1177/1045389X11412641)
22. Olympio KR, Gandhi F. 2010 Flexible skins for morphing aircraft using cellular honeycomb cores. *J. Intell. Mater. Syst. Struct.* **21**, 1719–1735. (doi:10.1177/1045389X09350331)
23. Reed Jr JL, Hemmelgarn CD, Pelley BM, Havens E. 2005 Adaptive wing structures. *Proc. SPIE.* **5762**, 133. (doi:10.1117/12.599922)
24. Spadoni A, Ruzzene M. 2007 Static aeroelastic response of chiral-core airfoils. *J. Intell. Mater. Syst. Struct.* **18**, 1067–1075. (doi:10.1177/1045389X06072361)
25. Ju J, Ananthasayanam B, Summers JD, Joseph P. 2010 Design of cellular shear bands of a non-pneumatic tire—investigation of contact pressure. *SAE Int. J. Passenger Cars-Mech. Syst.* **3**, 598–606.
26. Ju J, Kim D-M, Kim K. 2012 Flexible cellular solid spokes of a non-pneumatic tire. *Compos. Struct.* **94**, 2285–2295. (doi:10.1016/j.compstruct.2011.12.022)
27. Guo CY, Wheeler L. 2006 Extreme Poisson's ratios and related elastic crystal properties. *J. Mech. Phys. Solids* **54**, 690–707. (doi:10.1016/j.jmps.2005.11.002)
28. Evans K. 1991 The design of doubly curved sandwich panels with honeycomb cores. *Compos. Struct.* **17**, 95–111. (doi:10.1016/0263-8223(91)90064-6)



29. Ruzzene M. 2004 Vibration and sound radiation of sandwich beams with honeycomb truss core. *J. Sound Vib.* **277**, 741–763. (doi:10.1016/j.jsv.2003.09.026)
30. Ruzzene M, Scarpa F. 2005 Directional and band-gap behavior of periodic auxetic lattices. *Phys. Status Solidi B* **242**, 665–680. (doi:10.1002/pssb.200460385)
31. Scarpa F, Tomlinson G. 2000 Theoretical characteristics of the vibration of sandwich plates with in-plane negative Poisson's ratio values. *J. Sound Vib.* **230**, 45–67. (doi:10.1006/j.jsv.1999.2600)
32. Ajdari A, Jahromi BH, Papadopoulos J, Nayeb-Hashemi H, Vaziri A. 2012 Hierarchical honeycombs with tailorable properties. *Int. J. Solids Struct.* **49**, 1413–1419. (doi:10.1016/j.ijsolstr.2012.02.029)
33. Christensen R. 1987 Sufficient symmetry conditions for isotropy of the elastic moduli tensor. *J. Appl. Mech.* **54**, 772. (doi:10.1115/1.3173115)
34. Bertoldi K, Boyce M, Deschanel S, Prange S, Mullin T. 2008 Mechanics of deformation-triggered pattern transformations and superelastic behavior in periodic elastomeric structures. *J. Mech. Phys. Solids* **56**, 2642–2668. (doi:10.1016/j.jmps.2008.03.006)
35. Bertoldi K, Reis PM, Willshaw S, Mullin T. 2010 Negative Poisson's ratio behavior induced by an elastic instability. *Adv. Mater.* **22**, 361–366. (doi:10.1002/adma.200901956)
36. Gibson L, Ashby M, Schajer G, Robertson C. 1982 The mechanics of two-dimensional cellular materials. *Proc. R. Soc. Lond. A* **382**, 25–42. (doi:10.1098/rspa.1982.0087)
37. Gibson L, Ashby M, Zhang J, Triantafillou T. 1989 Failure surfaces for cellular materials under multiaxial loads—I. Modelling. *Int. J. Mech. Sci.* **31**, 635–663. (doi:10.1016/S0020-7403(89)80001-3)
38. Chen WF, Han DJ, Han D. 2007 *Plasticity for structural engineers*. Plantation, FL: J Ross Publication.
39. Gibson LJ, Ashby MF. 1999 *Cellular solids: structure and properties*. Cambridge, UK: Cambridge University Press.